Available online at www.sciencedirect.com
ScienceDirect
Journal of Sound and Vibration 302 (2007) 457–470
JOURNAL OF SOUND AND VIBRATION
www.elsevier.com/locate/jsvi

The use and limitations of continuum modes for response calculations of cellular structures

Sourish Banerjee[a], Atul Bhaskar[b,*]

[a]*Centre for Advanced Composite Materials, Department of Mechanical Engineering, The University of Auckland, Auckland, New Zealand*
[b]*School of Engineering Sciences, University of Southampton, SO17 1BJ, UK*

Received 28 September 2005; received in revised form 28 July 2006; accepted 8 September 2006
Available online 25 January 2007

Abstract

In this paper, a method for the approximate calculations of response of cellular structures is presented. The method is based on the idea that for low-frequency modes, the cellular structures behave in a way similar as a continuum does. The range of validity of the method on the mode number scale is also examined. It is shown that the response is estimated very accurately from a reduced order model based on continuum modes for low-frequency vibration. The accuracy starts to deteriorate with the increase in the mode number. Beyond certain mode number, the improvement in accuracy due to the inclusion of additional continuum modes in the approximation shows a point of diminishing returns. Illustrative examples are given.

1. Introduction

Numerous natural and engineered materials possess cellular internal structure. Common examples are bone, wood, structured ceramics, and metallic or polymeric foams. The mechanics of this class of materials has been studied extensively under static loading in the elastic and plastic regimes. For example, Gibson et al. [1] presented expressions for the elastic moduli of planar foams having hexagonal cell geometry using a unit cell approach. Gulati [2] derived these properties for foams having triangular cells using an energy approach. Scarpa et al. [3] studied auxetic foams computationally as well as experimentally. Other mechanical problems such as those involving plasticity, buckling, thermal conductivity, etc. are presented in the book authored by Gibson et al. [4]. The variability of mechanical properties, their dependence on micro-structural variability, and the effect of imperfections have been studied by several researchers (see, for example, Refs. [5–9]). With the exception of Wang and Stronge [10], who used a micro-polar theory to study response under fluctuating loads, research in the area of dynamics of cellular material is very limited.

In a recent paper [11], we presented a method based on the so-called continuum modes to calculate the natural frequencies of a structure made of cellular material in a computationally efficient way. It was remarked there that the method is suitable for low mode number calculations. This method is extended to response

*Corresponding author.
E-mail address: A.Bhaskar@soton.ac.uk (A. Bhaskar).

0022-460X/$ - see front matter © 2006 Elsevier Ltd. All rights reserved.
doi:10.1016/j.jsv.2006.09.032

calculations in the present work. The limits of the applicability of this approach are computationally examined. It is shown that including more and more number of continuum modes in the basis for the assumed modes method has a point of diminishing returns. A Rayleigh damping term is included to bring realism into the response calculations. This choice of this damping model is guided purely by mathematical-computational convenience rather than any known physics.

An outline of the present paper is presented next. The equations of motion for the reduced order model are derived in the next section. The application of Lagrange's equations lead to a reduced order system with smaller stiffness, inertia and damping matrices in addition to the reduced order forcing vector. Numerical comparisons of the approximations brought about by model order reduction are presented in Section 3. The limitations on the frequency range are discussed in Section 4. Conclusions are drawn in Section 5.

2. Development of the reduced order model using the continuum modes

We will assume that a large-scale finite element model of a cellular structure is given to us. The model possesses N degrees-of-freedom. The governing equations of motion take the form

$$\mathbf{M}\ddot{\mathbf{q}} + \mathbf{C}\dot{\mathbf{q}} + \mathbf{K}\mathbf{q} = \mathbf{f}, \tag{1}$$

where $\mathbf{K}$ is the stiffness matrix, $\mathbf{M}$ is the mass matrix, $\mathbf{f}$ is the force vector, and $\mathbf{q}$ is the vector of generalised coordinates. Further, it is assumed that viscous damping matrix $\mathbf{C}$ of the whole model is available to us.

When the driving force is harmonic of the form $\mathbf{f} = \hat{\mathbf{f}}e^{j\omega t}$, then the response $\mathbf{q} = \hat{\mathbf{q}}e^{j\omega t}$ is harmonic too. The frequency response function matrix is given by

$$\mathbf{H}(\omega) = (-\omega^2\mathbf{M} + j\omega\mathbf{C} + \mathbf{K})^{-1}. \tag{2}$$

The size of $\mathbf{H}(\omega)$ matrix is $N \times N$ for each value of the driving frequency ω. Hence, the evaluation of $\mathbf{H}(\omega)$ is computationally demanding if N is large. In many practical cases, response for a particular degree-of-freedom is required. In those cases, the response $\mathbf{q}$ can be obtained by solving a set of linear algebraic equations, in the form $(-\omega^2\mathbf{M} + j\omega\mathbf{C} + \mathbf{K})\hat{\mathbf{q}} = \hat{\mathbf{f}}$, without explicitly inverting the matrix $(-\omega^2\mathbf{M} + j\omega\mathbf{C} + \mathbf{K})$. This too is an expensive calculation.

In order to reduce the computational expense associated with response calculations, a reduced order model with p number of pre-conditioned assumed modes will be built, where $p \ll N$. Model order reduction will be achieved by the use of the so-called continuum modes [11] as the basis modes. Free vibration calculations were presented in Ref. [11] and it was shown that fairly accurate approximations for the natural frequencies can be obtained. Response predictions, on the other hand, may not be accurate despite accurate frequency predictions. An indication of the quality of prediction for the frequency response did come in Ref. [11] from the modal assurance criterion (MAC) plots, because frequency response combines the natural frequency and mode shape informations. However, it is unclear at this stage as to how accurate the effective damping ratios will turn out to be as a result of the model order reduction process. Finally, the limitations of the applicability of the continuum modes as basis modes were qualitatively suggested in Ref. [11]: we explore its validity computationally in the present paper.

Let us assume that the motion of the structure at any time t can be approximated by the superposition of p number of assumed modes as

$$\boldsymbol{\phi}(t) = a_1\boldsymbol{\psi}_1 + a_2\boldsymbol{\psi}_2 + \cdots + a_p\boldsymbol{\psi}_p, \quad p \ll N, \tag{3}$$

where $a_1, a_2, \ldots, a_p$ are time-dependent generalised coordinates of the structure. The basis modes $\boldsymbol{\psi}_i, i = 1, 2, \ldots, p$ are calculated based on the so-called *continuum modes*. In Section 2 of Ref. [11], an approximation for the cellular structures was developed based on the physical reasoning that for low-frequency dynamics, the overall mode shape of a cellular structure can be guessed by considering the structure as homogeneous. The mode shapes of such hypothetical porosity filled medium were referred to as continuum modes. The displacement and the rotation of each joint of the cellular model were then calculated by a kinematic mapping of the displacement and the rotation field of the cheaply calculated free vibration modes onto the corresponding point of the cellular structure.

A direct use of the assumed modes $\boldsymbol{\psi}_i$ as a basis fails to predict the natural frequencies and the mode shapes accurately [11, Section 3]. This is due to the presence of the exceptionally high-frequency components in the trial modes as identified in Ref. [11]. Hence, a method of pre-conditioning based on the inverse power iterations was proposed to filter them out. This difficulty is encountered in the present study too—for frequency response calculations—and is resolved by using a similar pre-conditioning strategy. The pre-conditioned assumed modes obtained thus are used here in approximation (3) for predicting the response of the cellular structures in a computationally efficient way.

The expansion (3) can be expressed as a transformation

$$\boldsymbol{\phi}(t) = \mathbf{T}\mathbf{a}(t), \tag{4}$$

where $\mathbf{T}$ is the transformation matrix of size $N \times p$, whose columns are the assumed modes $\boldsymbol{\psi}_i$, $i = 1, 2, \ldots, p$:

$$\mathbf{T} = [\boldsymbol{\psi}_1 | \boldsymbol{\psi}_2 | \cdots | \boldsymbol{\psi}_p] \tag{5}$$

and $\mathbf{a}$ is a column of unknowns $a_1, a_2, \ldots, a_p$. Note that the transformation matrix $\mathbf{T}$ has a structure similar to that of the modal matrix but it contains only p number of modes. In addition, these p modes are only approximate unlike the modal matrix where they are exact and complete.

The kinetic energy $T(t)$ and the potential energy $V(t)$ of the whole structure can be expressed as $T(t) = \frac{1}{2}\dot{\boldsymbol{\phi}}^{\mathrm{T}}\mathbf{M}\dot{\boldsymbol{\phi}}$, $V(t) = \frac{1}{2}\boldsymbol{\phi}^{\mathrm{T}}\mathbf{K}\boldsymbol{\phi}$. Substituting transformation (4) into the expressions of T and V and simplifying, we obtain

$$T(t) = \tfrac{1}{2}\dot{\mathbf{a}}^{\mathrm{T}}\overline{\mathbf{M}}\dot{\mathbf{a}}, \quad V(t) = \tfrac{1}{2}\mathbf{a}^{\mathrm{T}}\overline{\mathbf{K}}\mathbf{a}, \tag{6}$$

where $\overline{\mathbf{M}} = \mathbf{T}^{\mathrm{T}}\mathbf{M}\mathbf{T}$ and $\overline{\mathbf{K}} = \mathbf{T}^{\mathrm{T}}\mathbf{K}\mathbf{T}$. The matrices $\overline{\mathbf{K}}$ and $\overline{\mathbf{M}}$ will be referred to as the reduced stiffness and the inertia matrices, respectively, because of their reduced size $p \times p$.

Damping, assumed to be derivable from the Rayleigh's dissipation function, can be expressed similarly as $\mathscr{F} = \frac{1}{2}\dot{\boldsymbol{\phi}}^{\mathrm{T}}\mathbf{C}\dot{\boldsymbol{\phi}}$. Using transformation (4), this expression reduces to

$$\mathscr{F} = \tfrac{1}{2}\dot{\mathbf{a}}^{\mathrm{T}}\overline{\mathbf{C}}\dot{\mathbf{a}}, \tag{7}$$

where $\overline{\mathbf{C}}$ is the reduced damping matrix of size $p \times p$. If $\overline{\mathbf{Q}}$ is the generalised viscous damping force for the reduced model, then it can be derived from the Rayleigh's dissipation function as

$$\overline{Q}_r = -\frac{\partial \mathscr{F}}{\partial \dot{a}_r}, \quad r = 1, 2, \ldots, p. \tag{8}$$

The variation of the non-conservative work done by all other forces other than the viscous forces (for the full model) is expressed as

$$\delta W_{nc} = \sum_{r=1}^{N} f_r \delta\phi_r = \sum_{r=1}^{N} f_r \left(\sum_{s=1}^{p} T_{rs}\delta a_s \right). \tag{9}$$

If $\overline{\mathbf{f}}$ is the vector of the generalised forces corresponding to the reduced model of the structure producing the generalised displacements $\mathbf{a}$, then the variation of the non-conservative work done is given by $\delta W_{nc} = \sum_{s=1}^{p} \overline{f}_s \delta a_s$. Since the virtual work done is the same for both the systems, we obtain,

$$\overline{f}_s = \sum_{r=1}^{N} f_r T_{rs}, \quad s = 1, 2, \ldots, p. \tag{10}$$

Lagrange's equation of motion in terms of the new set of generalised coordinates and generalised forces, a_i and $\overline{f}_i$, can be written as

$$\frac{\mathrm{d}}{\mathrm{d}t}\left(\frac{\partial L}{\partial \dot{a}_i}\right) - \frac{\partial L}{\partial a_i} + \frac{\partial \mathscr{F}}{\partial \dot{a}_i} = \overline{f}_i, \quad i = 1, 2, \ldots, p, \tag{11}$$

where $L = T - V$ is the Lagrangian of the structure.

Substituting expressions of Eq. (6) into Eq. (11), we obtain the set of reduced order equations of motion in the matrix form as $\overline{\mathbf{M}}\ddot{\mathbf{a}} + \overline{\mathbf{C}}\dot{\mathbf{a}} + \overline{\mathbf{K}}\mathbf{a} = \overline{\mathbf{f}}$.

If the generalised force $\overline{\mathbf{f}}$ is of the form $\overline{\mathbf{f}} = \hat{\mathbf{f}}_{\text{red}} e^{j\omega t}$—the subscript indicating that it refers to the forcing vector of the reduced order model—then the generalised response $\mathbf{a} = \hat{\mathbf{a}} e^{j\omega t}$. Substituting for $\overline{\mathbf{f}}$ and $\mathbf{a}$ in the reduced order equations of motion, we have $\hat{\mathbf{a}} = (-\omega^2\overline{\mathbf{M}} + j\omega\overline{\mathbf{C}} + \overline{\mathbf{K}})^{-1}\hat{\mathbf{f}}_{\text{red}}$, where the coefficient matrix on the right side is similar to the previous expression (2). Hence, the reduced order frequency response function matrix is given by

$$\overline{\mathbf{H}}(\omega) = (-\omega^2\overline{\mathbf{M}} + j\omega\overline{\mathbf{C}} + \overline{\mathbf{K}})^{-1}. \tag{12}$$

The coefficient matrices $\overline{\mathbf{M}}$, $\overline{\mathbf{K}}$ and $\overline{\mathbf{C}}$ are of size $p \times p$, which is much smaller than the original size $N \times N$, if we are interested in a frequency band spanned by the first few frequencies. Therefore, the calculation of $\overline{\mathbf{H}}(\omega)$ needs much less computational effort than evaluating $\mathbf{H}(\omega)$. The displacement field at each node of the cellular structure $\boldsymbol{\phi}$ can be calculated from Eq. (3) after evaluating the values of the a's.

2.1. Proportional damping

It is extremely difficult to measure the damping of individual cell walls of cellular matter such as foam. In the absence of any damping model for the constituent parts, proportional or classical damping has been used in this paper. Expressing the damping matrix as a linear combination of the stiffness matrix and the mass matrix, we have $\mathbf{C} = \alpha\mathbf{M} + \beta\mathbf{K}$. Substituting for $\mathbf{C}$ and $\boldsymbol{\phi}$ into $\mathscr{F} = \frac{1}{2}\dot{\boldsymbol{\phi}}^{\mathrm{T}}\mathbf{C}\dot{\boldsymbol{\phi}}$, and simplifying, the expression for Rayleigh's dissipation function becomes

$$\mathscr{F} = \tfrac{1}{2}\dot{\mathbf{a}}^{\mathrm{T}}(\alpha\overline{\mathbf{M}} + \beta\overline{\mathbf{K}})\dot{\mathbf{a}}. \tag{13}$$

Comparing this with Eq. (7), the reduced order damping matrix is obtained as $\overline{\mathbf{C}} = \alpha\overline{\mathbf{M}} + \beta\overline{\mathbf{K}}$.

A commonly encountered difficulty while using the Rayleigh damping model is the lack of a rational approach to obtain the damping coefficients α and β. In this paper, calculations based on *prescribed* values of the damping ratio at the terminal points of the frequency band of interest are used.

The eigenvectors $\mathbf{u}$ for the structure can be calculated solving the eigenvalue problem $\mathbf{K}\mathbf{u}_r = \lambda_r\mathbf{M}\mathbf{u}_r$ associated with the undamped problem. The eigenvectors are stacked to obtain the modal matrix as $\mathbf{U} = [\mathbf{u}_1|\mathbf{u}_2|\cdots|\mathbf{u}_N]$. If the eigenvectors are orthonormal, then they satisfy the orthogonality relations $\mathbf{U}^{\mathrm{T}}\mathbf{M}\mathbf{U} = \mathbf{I}, \mathbf{U}^{\mathrm{T}}\mathbf{K}\mathbf{U} = \text{diag}[\omega_r^2], r = 1, 2, \ldots, N$. For proportional damping, $\mathbf{U}^{\mathrm{T}}\mathbf{C}\mathbf{U}$ is a diagonal matrix and is given by

$$\mathbf{U}^{\mathrm{T}}\mathbf{C}\mathbf{U} = \text{diag}[2\zeta_r\omega_r] = \alpha\mathbf{I} + \beta\,\text{diag}[\omega_r^2], \quad r = 1, 2, \ldots, N, \tag{14}$$

where ζ_r is the damping ratio for the rth mode. Therefore the modal damping ratios are given by $\zeta_r = (\alpha/2\omega_r) + (\beta\omega_r/2), r = 1, 2, \ldots, N$. If the value of ζ is specified at the two extremes of a frequency band, then we obtain two equations for the unknowns α and β. Solving for these unknowns we obtain the two parameters required in the Rayleigh damping model.

Carrying out algebra on the lines of the arguments in the last paragraph (but for expressions corresponding to the reduced order model), we obtain the damping ratios for the reduced model as

$$\overline{\zeta}_r = \frac{\alpha}{2\overline{\omega}_r} + \frac{\beta\overline{\omega}_r}{2}, \quad r = 1, 2, \ldots, p, \tag{15}$$

where $\overline{\zeta}_r$ and $\overline{\omega}_r$ denote the damping ratio and the natural frequency corresponding to the rth mode of the reduced model. The above expression is used here for the determination of the damping ratios as predicted by the reduced order model. This expression shows that the quality of estimates for the damping ratio depends upon the accuracy of the natural frequencies predicted by the reduced order model.

3. A numerical example and discussions

The cantilever beam, fixed at the left end and free at the right end as shown in Fig. 1, is taken up now to illustrate the continuum model based calculations of the frequency response. The geometric and the material data of the beam are presented in Table 1. The global stiffness matrix $\mathbf{K}$ and the global inertia matrix $\mathbf{M}$ of the beam are assembled in the usual way. The model used here is the same as that in Ref. [11] and the continuum

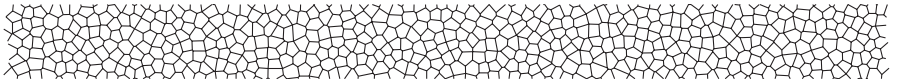

Fig. 1. A cellular beam made of irregular cells. The beam vibrates in the plane of the paper.

Table 1
Geometric and material data for the beam shown in Fig. 1

Length of the model L	600 mm
Overall depth in the transverse direction D	50 mm
Length of the cell wall material $\sum_i l_i$	7575.4 mm
Thickness of the each cell wall t	0.175 mm
Number of nodes	1148
Number of elements	1556
Material data	
Cell walls are made of aluminium	
Young's modulus E_s	70 GPa
Density ρ_s	2700 kg/m^3

free vibration modes were obtained as in Ref. [11]. These continuum modes were evaluated from the finite element analysis of the single fixed–free beam having the same macroscopic dimensions as the cellular beam. The assumed modes were calculated from these modes through mapping on the lines of Eq. (6) of Ref. [11] using Eqs. (4) and (5) therein. These assumed modes were chosen as the basis modes after pre-conditioning using Eq. (29) of Ref. [11].

The basis modes were used for model order reduction. Frequency response calculations were carried out by using the coefficient matrices of the original model and the reduced order model. The undamped response is considered in the next sub-section, followed by the damped response in the subsequent sub-section.

3.1. Undamped response

A transverse harmonic force $\hat{\mathbf{f}}e^{j\omega t}$ is applied to a node near the 'neutral axis' of the macroscopic beam since it is practically not possible to find a node on the neutral axis when irregular cells are present. The coefficient matrices and the force vector for the reduced model $\overline{\mathbf{K}}$, $\overline{\mathbf{M}}$ and $\overline{\mathbf{f}}$ are calculated using Eqs. (6) and (10). The unknowns a_r are determined by solving $\hat{\mathbf{a}} = (-\omega^2\overline{\mathbf{M}} + j\omega\overline{\mathbf{C}} + \overline{\mathbf{K}})^{-1}\hat{\mathbf{f}}_{\text{red}}$, without explicit inversion. The complete displacement field is obtained by the transformation (3) after substituting the values of a_r. The driving point and the transfer receptances of the reduced order model are compared with those obtained from the full scale finite element simulations.

The vertical displacement of a point due to a harmonic vertical load is calculated. The amplitude of the driving point receptance calculated from the full scale model is compared with the calculations based on the reduced order model in Fig. 2. The frequency band chosen here contains ten modes of the finite element model. The driving point response shows similar features as is observed in the case of a homogeneous continuum. The finite height of the peaks is due to the finite resolution of the frequency stepping. The figure shows an excellent agreement—the error in frequency calculation being less than 1% up to the ninth mode (the ninth mode appears as the eighth peak in Fig. 2 because the mode corresponding to axial motion is missing in this transverse driving point calculation). The response curve starts deviating progressively after the ninth peak. The tenth frequency estimated by the reduced model is higher by 7% than the corresponding value calculated by the full scale finite element analysis. The accuracy of the tenth frequency can be improved by including more number of basis modes instead of including only ten. This, and the limits to the improvements, will be studied in Section 4.

It is expected that the overall motion of the structure will be primarily vertical when the load is applied vertically. This can lead to missing modes that are associated with non-vertical motion. Fig. 2 shows the axial

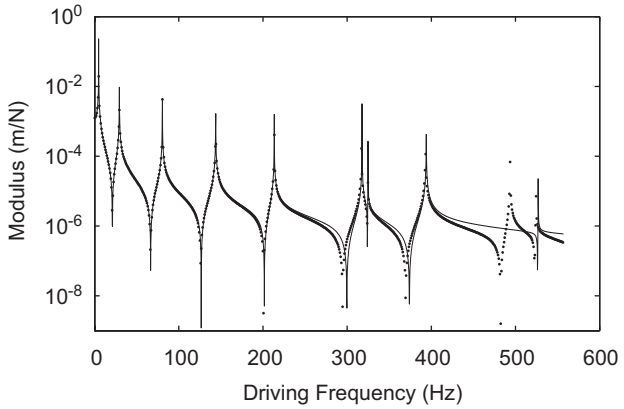

Fig. 2. Driving point receptance with zero damping as calculated due to a harmonic vertical load acting at a right hand boundary node. Legend: — reduced order model, · full scale model using finite element analysis. Note that the peak associated with the first *axial* mode between the third and the fourth peaks is missing.

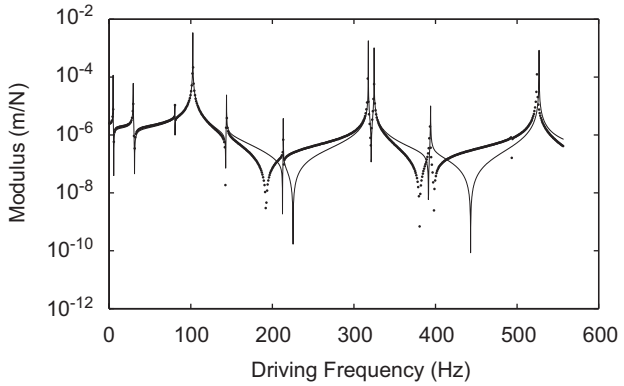

Fig. 3. Undamped driving point response when a harmonic axial load acts at the same node as Fig. 2. Legend: — reduced model, · FE. Sharp resonance peaks are observed at the frequencies corresponding to the axial modes. The first axial mode missing in Fig. 2 is prominent now.

mode between the third and the fourth peaks at 102.51 Hz missing. On the other hand, the sixth peak in this figure corresponds to an axial mode which is possibly due to small bending axial mode coupling afforded by the irregular micro-structure. There is an anti-resonance between any two resonances in Fig. 2. This is characteristic of a driving point response.

The driving point receptance due to *axial* loading is presented next. Fig. 3 shows the comparisons of the amplitude of the point receptance as calculated from the full scale finite element analysis and the reduced order model. The agreement is generally good. Note that the axial mode missing in Fig. 2 at 102.51 Hz is the dominant peak now. Peaks associated with the axial modes are more pronounced now. Small resonance peaks associated with the flexural modes are observed in addition to the axial modes. This can be attributed to small coupling introduced by the irregularity.

The transfer receptance is calculated next when the driving point is unchanged and the response point is a joint close to the centre of the sample (coordinates 30.56, 5.36 mm). Driving as well as the transfer response are in the vertical direction (Fig. 4). The agreement between the full scale model and the reduced order model is again very good up to the ninth mode.

The spatial response of the structure as estimated by the reduced order model will be compared with that from the full model next. Frequency domain assurance criterion (FDAC) is used here for correlating the

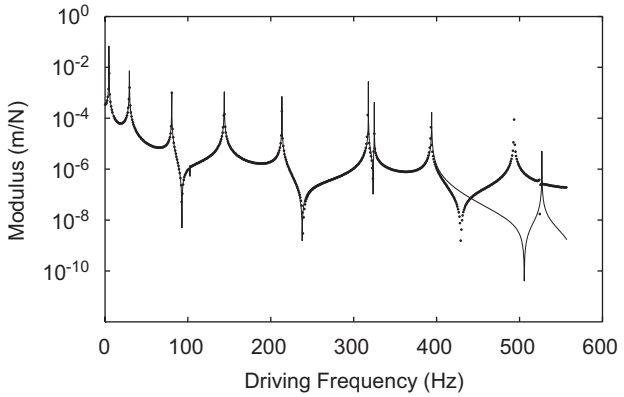

Fig. 4. Undamped transfer receptance due to a vertical load applied at the same driving point as before. Legend: — reduced model, · FE. Note the absence of the anti-resonances between the resonance peaks in many cases. This is a characteristic of transfer receptance.

response vectors $\boldsymbol{\phi}$ and $\mathbf{q}$ in the frequency domain. The plot is similar to the MAC plot used in our previous paper [11] for comparing the eigenvectors. In the present case, it is impossible to compare the vectors at all the possible values of the driving frequency. Hence, the response functions are calculated at a set of chosen representative frequencies only. In this paper, the calculations are performed for all the natural frequencies and the mid-points between two adjacent modes on the frequency axis. The frequency band considered here has the first ten modes of the full scale model. Therefore, 20 pairs of vectors, $\boldsymbol{\phi}$ and $\mathbf{q}$ are generated for the FDAC plot.

The FDAC matrix $\mathbf{F}$ has the entries given by [12]

$$F_{rs} = \frac{|\mathbf{q}_r^{\mathrm{T}} \boldsymbol{\phi}_s^*|^2}{(\mathbf{q}_r^{\mathrm{T}} \mathbf{q}_r^*)(\boldsymbol{\phi}_s^{\mathrm{T}} \boldsymbol{\phi}_s^*)}. \tag{16}$$

The asterisk denotes the complex conjugate. In the absence of damping, the response vectors are real. Fig. 5 shows the relative magnitudes of F_{rs} for the pair of response vectors on a suitable grey-scale. The dark diagonal cells on this plot show excellent correlation between the spatial response as calculated by the full scale model and that as estimated by the reduced order model.

In order to assess computational savings, the number of floating point operations involved in both the approximate method and the finite element method are calculated when a vertical load is applied at a boundary node. A frequency interval of 0.16 Hz is considered which involves calculation of the response vector (3444×1), 3500 times. The total floating point operations required for calculations using the reduced model and the finite element model are 2.61×10^8 and 2.63×10^{10}, respectively. Therefore, the flops for the reduced model are only about 1% of those required for the full scale model. Note that the flop counts for the reduced model includes the generation of the assumed modes, the modes of the skeleton and preconditioning, etc. The assembly of the coefficient matrices is included in both cases of flop count calculation.

3.2. Damped response

The model analysed in the previous section is taken up now when damping is included in the model via Rayleigh damping. It is unclear how the damping ratios will be predicted when the model order reduction scheme proposed in our previous paper [11] is employed. Potentially, a mismatch in the effective damping ratio can seriously affect response near the resonances.

The value of the damping ratio ζ is taken as 1% for the first and the tenth mode. The values of the constants α and β are then calculated by solving two simultaneous equations for this chosen value of ζ in the expression for the modal damping ratios. The values of α and β evaluated as above are 0.596 and $6.39 \times 10^{-6}\,\mathrm{s}^{-1}$,

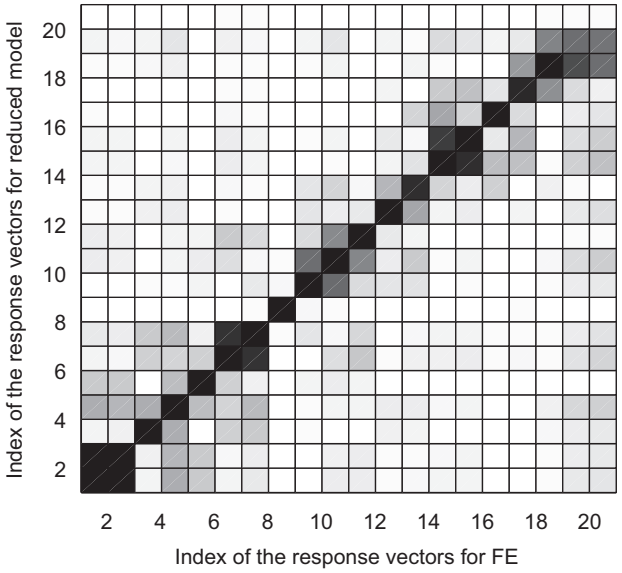

Fig. 5. FDAC plot representing correlation between the response vectors as calculated by the finite element simulations and the reduced model. The dark blocks on the diagonal show excellent correlation up to the ninth mode.

respectively. The reduced damping matrix $\overline{\mathbf{C}}$ is then generated as $\alpha\overline{\mathbf{M}} + \beta\overline{\mathbf{K}}$. The response is calculated from $\hat{\mathbf{a}} = (-\omega^2\overline{\mathbf{M}} + \mathrm{j}\omega\overline{\mathbf{C}} + \overline{\mathbf{K}})^{-1}\hat{\mathbf{f}}_{\mathrm{red}}$.

The point receptance is presented in Fig. 6 when a vertical point load is applied to a node close to the centre line. The agreement is excellent up to the ninth mode. This shows that the reduced damping matrix accurately captures the damping behaviour of the full scale model. The seventh mode is an axial mode which is also reproduced by the reduced order model since the basis modes include the axial continuum mode. Again, anti-resonances are observed between any two resonance peaks—a characteristic of driving point response. The phase is also reproduced accurately by the reduced order model (the bottom plot in Fig. 6). When damping is included in the model, the results (not shown here) have a general trend very similar to the one shown in Fig. 5.

The values of ζ and $\overline{\zeta}$, the damping ratios for the full scale model and that for the reduced order model, are plotted in Fig. 7. The figure shows that the damping ratios are well predicted by the reduced model up to the ninth mode. Note that the values for the first mode appear on the y-axis of the figure and corresponds to mode 1.

The total floating point operations required for the full scale and the reduced model calculations are 1.03×10^{11} and 9.99×10^{8}, respectively. Therefore, flops for the reduced model are less than 1% of that for the full model. The computational savings will be even greater when more number of response functions are to be calculated and when the size of the problem is larger.

It is shown in Fig. 5 that for the response calculation within a frequency band up to the tenth frequency, the correlation between the FE and the approximate response starts deteriorating rapidly after the ninth frequency when only ten modes are considered as a basis. To improve the accuracy further upto the frequency scale, more number of basis modes are to be included in the approximation. Error norms can be used as a measure of accuracy in this case. If $\boldsymbol{\phi}_{10}$ and $\boldsymbol{\phi}_{11}$ are the approximate response vectors (damped case) calculated using ten and eleven continuum modes, respectively, then the error norm is given by $\|e_{11}\| = \|\boldsymbol{\phi}_{10} - \boldsymbol{\phi}_{11}\|$. Similarly, $\|e_{12}\|$ is the norm of the difference between $\boldsymbol{\phi}_{11}$ and $\boldsymbol{\phi}_{12}$. The norms can be calculated by including one extra modes each time and compared. In this case, values of the $\|e_{11}\|$, $\|e_{12}\|$, $\|e_{13}\|, \|e_{14}\|$ and $\|e_{15}\|$ are 0.0047, 0.00052, 0.00013, 0.00021, 0.0000036, respectively. It shows that the convergence is achieved when fifteen modes are included in the basis. The FDAC values obtained using Eq. (16) show excellent correlation between the approximate and the FE vectors when fifteen modes are included. The limitations of adding more modes for improving accuracy are discussed next.

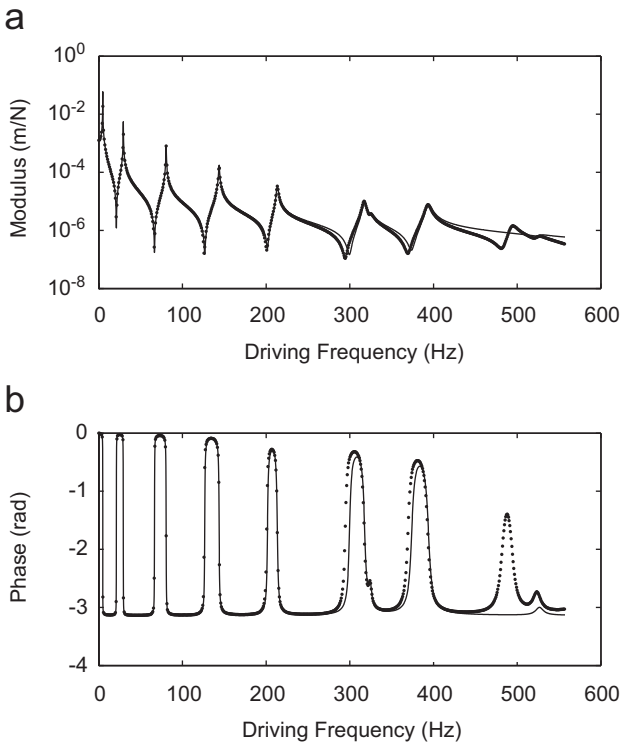

Fig. 6. Driving point receptance due to a vertical load. Damping is included in the model: (a) modulus plot: top and (b) phase plot: bottom. Legend: — reduced model, · FE. The response curves have the similar features as were observed in Fig. 2, with the difference is that the resonance peaks are now reduced due to damping.

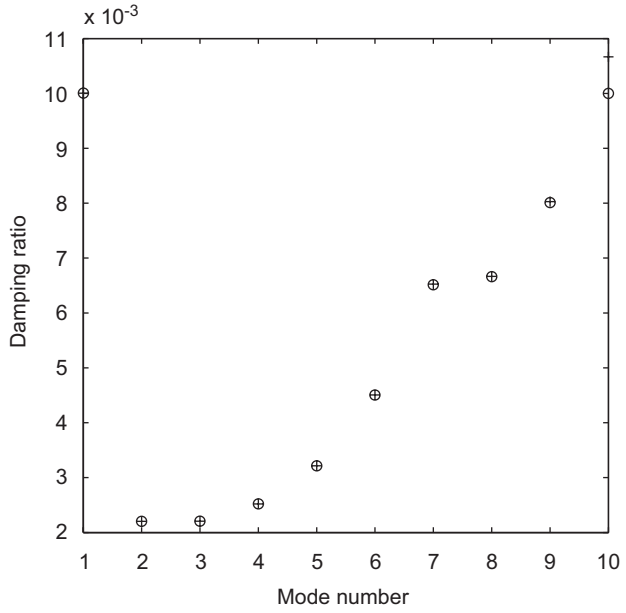

Fig. 7. A plot of the damping ratio (ζ_r) against mode number. Legend: + damping ratio from reduced model, ○ damping ratio from FE model. The ratios estimated on the basis of the reduced model are very accurate except for the last mode.

4. Limitations of the use of the continuum modes for response calculations

It was remarked earlier that the method presented in this paper and Ref. [11] are suitable for low-frequency calculations only. At high frequencies, the normal modes of a continuum of the same external shape as a piece of cellular solid will increasingly show differences with its cellular counterpart. Therefore, the approximation proposed in here and in Ref. [11] will break down because of progressively increasing importance of local details with mode number. In this section we explore these limitations.

The response calculations from the full scale finite element model and that calculated from the reduced order model are shown in Fig. 8 when the first 40 continuum modes are used for model order reduction. By including extra set of modes in the reduced model, the performance of approximations is enhanced up to a point. When we compare Figs. 6 and 8, we note that the mode around 500 Hz that is poorly captured by the reduced order model is now approximated very accurately. However, beyond about fourteen modes, inclusion of extra modes has little influence on the response prediction by the reduced order model. This trend in the magnitude plot—that the improvement in response calculation is only marginal beyond a certain frequency—is roughly observed in the phase plot as well.

There are two reasons for the failure of the continuum modes to produce accurate response beyond a band of frequency as shown in Fig. 8. Firstly, with increase in frequency, the mode shapes of a cellular structure increasingly differ from the mode shape that one would get if we filled the cellular medium with a continuum with some effective properties. The length scales relevant to this departure from the continuum behaviour are the wavelength (corresponding to a mode) and the size of a typical cell. Secondly, in the examples given here, the continuum modes were those of thin beam and thin rods in axial tension and compression. With increasing mode number, the wavelengths become shorter and the characteristic length starts becoming comparable to

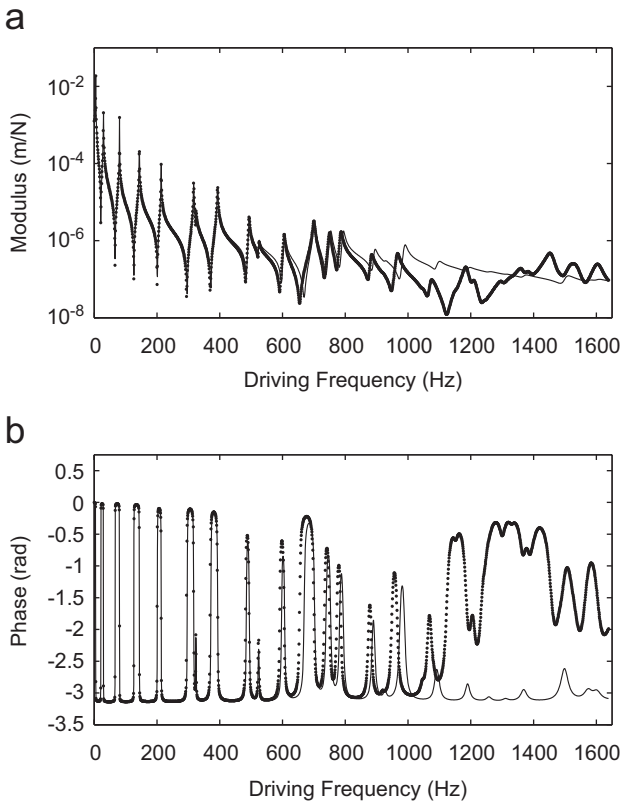

Fig. 8. Driving point damped FRF for the first 40 modes as predicted by the finite element simulations and the reduced order model: (a) modulus plot: top and (b) phase plot: bottom. Legend: — reduced model, · FE. The figure shows that after a certain mode number, inclusion of more basis modes fail to improve the predictions by the reduced model.

the overall depth of the beam—simple models of the continuum (such as a beam or a rod) break down—leading to the difficulty to faithfully represent the actual mode shape.

The above criterion can be used to estimate the limit of using the continuum modes in the proposed approximation. The characteristic length in the axial direction depends on the mode number and can be approximately taken as the distance between two nodes in a beam bending mode. When this characteristic length approaches the depth of the beam, beam theories become increasingly invalid. Beyond this mode number—up on the frequency scale—the proposed approximation is expected to become increasingly poor: thus affording a physics based limit to the applicability of the approximation. This scaling argument can now be applied to the numerical example presented in this paper for which $L/D = 12$. Recalling that the characteristic length in the axial direction for the Nth mode is approximately L/N (the modal spacing is not perfectly uniform for beam bending, but these subtleties can be ignored in a scaling argument), we conclude that the limit to the applicability of the proposed approximation is about the 12th beam bending mode. Accounting for the fact that we have four axial modes below the 12th bending mode, we expect the approximation to rapidly deteriorate above the 16th overall mode number. The actual value of frequency will, of course, depend on the dimensions and the material properties, but the above argument still provides a limit to the applicability of the approximation. The predicted limit of the applicability of the approximation is well-supported by the numerical calculations. Figs. 9–11 consistently show (for natural frequency, damping ratio and mode shape comparisons, respectively) that the approximation degrades rather rapidly beyond the 17th or the 18th mode.

The argument based on the characteristic length scale of a normal mode can be further used to assess the maximum number of terms to be used in the continuum modes approximation. Since the beam behaviour ceases when the wavelength is of the order of depth, it suggests that the approximation reaches a point of diminishing returns when more modes are included in the approximation. For the example discussed in the previous paragraph, the number of continuum mode terms is, therefore, not to exceed much beyond 16 terms. This is consistent with the observation made at the end of Section 3 that convergence in response was reached with 15 continuum modes. In practical situations, one may include a few extra modes to let the response near the highest predictable modes converge, but beyond those few extra modes—inclusion of further modes is pointless. This is supported by Fig. 11 when 40 modes are used: beyond the 18th mode, there is little improvement. These numerically observed mode numbers for the limit of applicability of the proposed method as well as the optimal number of terms to be included in the approximation—around the predicted mode

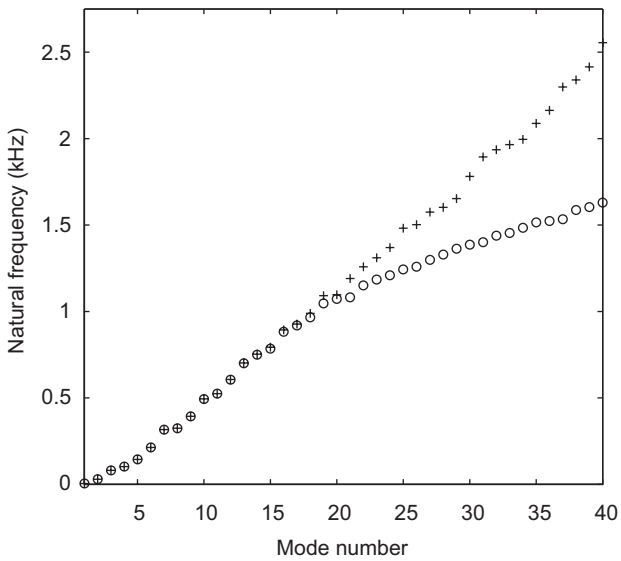

Fig. 9. The first 40 natural frequencies (ω_r) are plotted. Legend: + natural frequency from reduced model, ○ natural frequency from FE model. Note that the discrepancy between the values as calculated by the proposed reduced model and those from the finite element increases beyond a certain mode number even when more number of continuum modes are included in the basis.

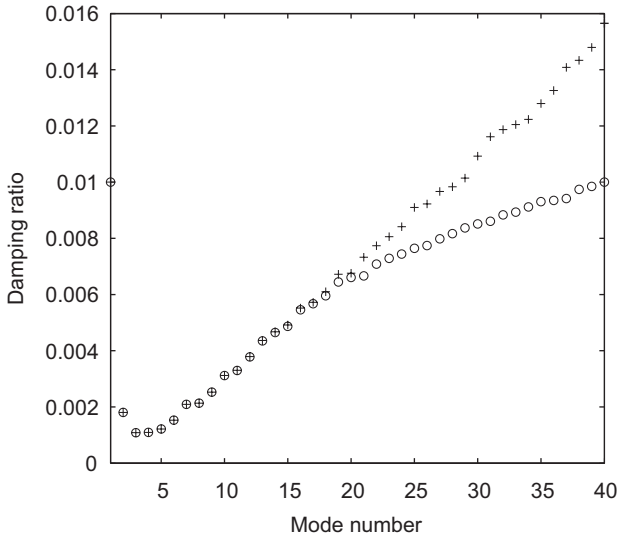

Fig. 10. The damping ratios (ζ_r) associated with the first 40 modes are plotted. Legend: + damping ratio from reduced model, ○ damping ratio from FE model. Note that the trend in the discrepancy between the values from the FE model and those from the reduced order model: at high mode number $2\zeta_r \sim \beta\omega_r$ and $2\bar{\zeta}_r \sim \beta\bar{\omega}_r$ which conforms with the trends in Fig. 9.

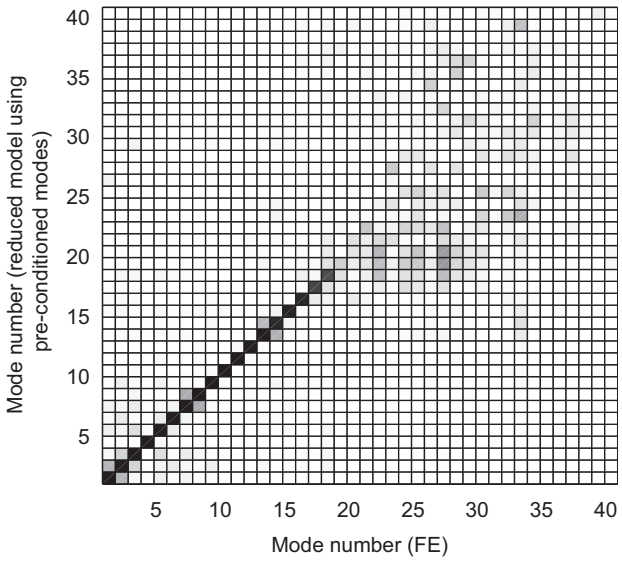

Fig. 11. FDAC plot representing correlation between the damped response vectors when 40 modes are used.

number 16—should be seen in the context that the overall degrees on freedom are well above 3000. Although the scaling argument is approximate, it gives a very good indication both for the validity of the method as well as the optimal number of terms to be used in the approximation.

It may be possible to extend the applicability of the proposed method by using modes of a better quality continuum model (such as plane stress). However, we have not employed any such method because the main purpose of the approximation—to save computations—starts being defeated because the cost of discretising the continuum (e.g. plane stress) to obtain the continuum modes computationally may be significant and the benefits of avoiding full scale computations having structural details at the cellular level may be only marginal.

The error in response calculations due to model order reduction can be seen in Fig. 8 at two levels. First, the positions of the peaks of the full scale computation and the reduced model show departure that increases with

frequency. Second, the response at high frequency appears to be greatly damped. The undamped natural frequencies as obtained from the full scale finite element model and the reduced order model are shown in Fig. 9. The errors progressively increase beyond about 15 modes. The damping ratios from the two models for various modes have been plotted in Fig. 10. As expected, the values are over-predicted by the reduced order calculations affecting the response calculations adversely.

The similarity in the trends for the discrepancies between the calculations from the full scale model and the reduced order model is striking. The reason is the choice of the Rayleigh damping model for which the asymptotic relations:

$$2\zeta_r \sim \alpha/\omega_r, \quad 2\overline{\zeta}_r \sim \alpha/\overline{\omega}_r$$

in the limit of low mode number, and

$$2\zeta_r \sim \beta\omega_r, \quad 2\overline{\zeta}_r \sim \beta\overline{\omega}_r$$

in the limit of high mode number, hold. In either of these two limiting cases, the relative errors are given by

$$\left|\frac{\mathrm{d}\zeta_r}{\zeta_r}\right| = \left|\frac{\mathrm{d}\omega_r}{\omega_r}\right|.$$

For the numerical example studied here, the relative error in the computed 40th natural frequency is about 57%; the corresponding error in the damping ratio is also about 57%.

The spatial correlation of response with an increased range of frequency is shown in Fig. 11. Note the breakdown of the correlation beyond mode number 18 in the FDAC plot of the full scale model vs. the reduced order model: the boxes on the diagonal cease to be dark indicating poor response correlation.

5. Conclusions

A method was proposed for the estimation of frequency response of cellular structures. The method makes use of the continuum modes as the set of basis functions for model order reduction on the lines of Ref. [11]. These modes needed pre-conditioning using an inverse power iteration. The response of the whole structure was predicted using the reduced order model.

A proportional damping model was used to include the effect of damping. The damping coefficients associated with the stiffness and the inertia matrices were calculated for a frequency bandwidth when the value of the damping ratio was prescribed for the two extremes of the band.

The response predicted by the proposed method was compared with that calculated from the full scale model for low-frequency vibration. The comparisons show good agreement for the damped as well as the undamped cases. The reduced order model predicts fairly accurate damping ratios for the first few modes. Without compromising the accuracy significantly, substantial computational saving is achieved when continuum modes are used for model order reduction.

The limitation of the proposed model order reduction is that it is suitable only for the low-frequency dynamics. This was demonstrated by considering calculations for an extended band of frequency. The correlation of frequency response, undamped natural frequencies, modal damping ratios, and spatial response show a limit to the applicability of the proposed model order reduction beyond which the quality of the approximation is inadequate. A scaling argument based on the characteristic wavelength of standing waves was presented to assess the range of the applicability of the proposed method.

Acknowledgments

This work was supported by the EPSRC Grant GR/R45895/01.

References

[1] L.J. Gibson, M.F. Ashby, G.S. Schajer, C.I. Robertson, The mechanics of two-dimensional cellular materials, *Proceedings of the Royal Society of London A* 382 (1982) 25–42.

[2] S.T. Gulati, Effects of cell geometry on thermal shock resistance of catalytic monoliths, *Automotive Engineering Congress and Exhibition Society of Automotive Engineers, Detroit*, Michigan, paper 750171, 1975, pp. 1–9.
[3] F. Scarpa, P. Panayiotou, G. Tomlinson, Numerical and experimental uniaxial loading on in-plane auxetic honeycombs, *Journal of Strain Analysis for Engineering Design* 35 (5) (2000) 383–388.
[4] L.J. Gibson, M.F. Ashby, *Cellular Solids: Structure and Properties*, second ed., Cambridge University Press, Cambridge, 1997.
[5] M.J. Silva, W.C. Hayes, L.J. Gibson, The effect of the non-periodic microstructure on the elastic properties of two-dimensional cellular solids, *International Journal of Mechanical Sciences* 37 (1995) 1161–1177.
[6] H.X. Zhu, J.R. Hobdell, A.H. Windle, Effects of cell irregularity on the elastic properties of 2D voronoi honeycombs, *Journal of The Mechanics and Physics of Solids* 49 (2001) 857–870.
[7] A.E. Simone, L.J. Gibson, Effects of solid distribution on the stiffness and strength of metallic foams, *Acta Materialia* 46 (1998) 2139–2150.
[8] J.L. Grenestedt, Influence of wavy perfections in cell walls on elastic stiffness of cellular solids, *Journal of The Mechanics and Physics of Solids* 46 (1998) 29–50.
[9] C. Chen, T.J. Lu, N.A. Fleck, Effect of imperfections on the yielding of two-dimensional foams, *Journal of The Mechanics and Physics of Solids* 47 (1999) 2235–2272.
[10] X.L. Wang, W.J. Stronge, Micropolar theory for a periodic force on the edge of elastic honeycomb, *International Journal of Engineering Sciences* 39 (2001) 821–850.
[11] S. Banerjee, A. Bhaskar, Free vibration of cellular structures using continuum modes, *Journal of Sound and Vibration* 287 (2005) 77–100.
[12] D.J. Ewins, *Testing, Theory, Practice and Applications*, second ed., Research Studies Press, Baldock Herts, 2000.